Improving the Accuracy of Droplet Measurement by Optical Fiber Probe Using 3D Ray-Tracing Simulation

In print. Journal of Chemical Engineering of Japan

Title

Improving the accuracy of droplet measurement by optical fiber probe using 3D ray-tracing simulation

Authors

Yuki Mizushima[1] and Takayuki Saito[2]

Affiliations

1) Graduate4 School of Science and Technology, Shizuoka University, 3-5-1 Johoku, Naka-ku, Hamamatsu, Shizuoka 432-8561, Japan

2) Corresponding author, Research Institute of Green Science and Technology, Shizuoka University, 3-5-1 Johoku, Naka-ku, Hamamatsu, Shizuoka 432-8561, Japan

E-mail: ttsaito@ipc.shizuoka.ac.jp

Phone and Fax: +81 53 478 1601

Keywords

Single-tip optical fiber probe, 3D ray-tracing simulation, Droplet, Post-signal, Measurement accuracy

Abstract

An optical fiber probe (OFP) is an intrusive but useful device for bubble/droplet measurement in gas-liquid two-phase flows. Although previous researchers have invented various types of OFP and established their own probe systems, few techniques have been

applied to measurements in practical machinery. In particular, successful examples of OFP for droplet measurement are extremely rare. We invented a single-tip OFP (S-TOP) for size/velocity measurement of submillimetre droplets. The difficulty of using S-TOP measurement in droplet flows, as is true with other OFPs and electric conductivity probes, is how to discriminate touch positions of the S-TOP on the droplet. To solve this difficult problem and improve the accuracy of the S-TOP, signal analysis of S-TOP was performed based on 3D ray tracing. Our ray-tracing simulation successfully revealed a very hopeful characteristic signal (named the post-signal) from a seemingly noisy peak; its intensity corresponded to the S-TOP's touch position. Based on this characteristic of the post-signal, we developed a method of signal processing for practical measurement of droplet velocity, chord length, and number density through the S-TOP. This new method considerably reduced the difference in the measured results between the chord lengths and velocities through the S-TOP and through visualization, to less than 10%.

1. Introduction

Spray atomization is an important engineering process; examples include fuel injection in gasoline/diesel engines, decontamination in healthcare environments, surface cleaning processes, and hot metal cooling. Improving the performance of spray atomizers is essential to reducing the discharge of greenhouse gases. For this specific purpose, a deep understanding of spray flows is needed. In hot metal cooling processes, for instance, the flow of cooling water through a control valve is a dense dispersed spray with rapidly changing spatial and temporal characteristics. To characterize these kinds of dispersed two-phase flows, several laser-based techniques, such as Phase Doppler Anemometry (PDA) (Sommerfeld 1993), Interferometric laser imaging (ILIDS) (Hess 1998; Kawaguchi et al. 2002) and optical fiber probe (Miller and Mitchie 1970) have been

developed to measure the size and velocity of droplets. Non-intrusive techniques like PDA and ILIDS, however, are not necessarily feasible for industrial measurements. For instance, PDA cannot observe droplets positioned deep inside the flow if the droplet number density is high. In such cases, droplets close to the detectors can easily blind the observation window, making measurements impossible due to the scattering of light.

Optical fiber probing (OFP) is an intrusive measurement; hence, it successfully detects droplets even if the number density is high. This optical measurement is almost free of electrical noise and intrinsic response time limitations compared to other phase detection techniques (resistance, capacitance, and thermal probes) (Cartellier 1991). It is adaptable not only for laboratory equipment but also for practical equipment. In OFP, one end of the fiber is usually a sensing tip that is smoothly ground by an abrasive plate, while the other end is connected to the optics. Laser beams propagated through the fiber reflect at the sensing tip, and some of the reflected beams are propagated back again through the same fiber. After reflection off a beam splitter, the return beams are detected by optical sensor. The returned light intensity depends on the difference in the refractive indices between the gas and liquid phase around the sensing tip; hence, the output signal is basically a type of on-off signal (Figure 1). From this on-off signal, various quantities, such as the velocities, sizes, number density, volumetric and number density fluxes, and interfacial area density, are calculated.

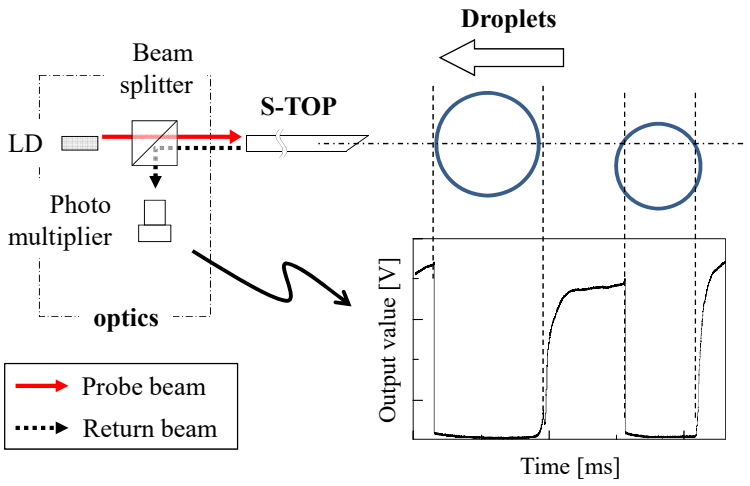

Figure 1. Schematic diagram of droplet measurement using an optical fiber probe.

OFPs are used extensively in bubbly flows (Abuaf et al. 1978; Aprin et al. 2007; Barrau et al. 1999; Harteveld 2005; Higuchi and Saito 2010; Vejratzka et al. 2010; Xue 2004). For droplet measurement, however, OFPs have rarely been employed. This is because the conventional type of multi-tip OFP is too large to pierce the small droplets (a few hundred micrometres or less in diameter) that commonly appear in droplet spray. Hong et al. (2004) studied how to simultaneously measure diameter, volumetric flux, and local liquid fraction of a 2D co-current planar liquid-gas jet (UG = 60 m/s, UL = 0.52 m/s) using a mono-fiber-optical probe, and concluded that the measurement uncertainty was within 15%. We independently developed a different type of mono-fiber-optical probe called the single-tip optical fiber probe (S-TOP), which is able to measure tiny droplets (Saito et al. 2009) using well-controlled conditions in terms of size, velocity, and trajectories of the droplets. The measurement range for velocity is up to 20 m/s, and the one for equivalent diameter is from 50–200 μm. The difference in average values between the S-TOP and visualization is less than 10%.

Although droplet measurement using the S-TOP under well-controlled conditions was successful, we could not estimate probable values of the velocity and size of droplets in three-dimensional (3D) dispersed flows. In Fig. 1, for example, droplet size is evaluated from a dwelling time (the time when the probe tip is positioned in a droplet), resulting in the pierced chord length as a droplet axis. However, the chord length is not necessarily equal to the droplet minor axis; it will vary depending on the pierced position. Moreover, it is impossible to discriminate pierced positions by existing signal processing. If we could directly detect the pierced position from the signal, droplets in a dispersed spray could be successfully measured with a high degree of accuracy. Our challenging new method utilizes a “post-signal” that appears before the S-TOP pierces a droplet’s rear surface (see Figure 3 [a]).

The aim of the present study is to improve the accuracy of droplet measurement using the S-TOP. Our 3D ray-tracing simulation (Sakamoto and Saito 2012) analyses a droplet signal of the S-TOP, and reveals physical meanings hidden in the signal. Combined with experimental results, we found that a post-signal intensity closely relates to the pierced position. We thus propose a post-signal method for direct detection of the pierced position, and discuss its effectiveness.

2. Single-tip optical fiber probe (S-TOP)

Figure 2 shows the S-TOP used in the present study. The S-TOP was composed of a synthetic silica optical fiber (external diameter, 230 μm; core diameter, 190 μm; cladding thickness, 15 μm; core refractive index, 1.46). The silica optical fiber was sharpened using a micropipette puller (P-2000, Sutter Instrument Company). The tip was subsequently cut into a wedge shape with an angle of 30° to the fiber axis by a micropipette beveller (BV-10, Sutter Instrument Company).

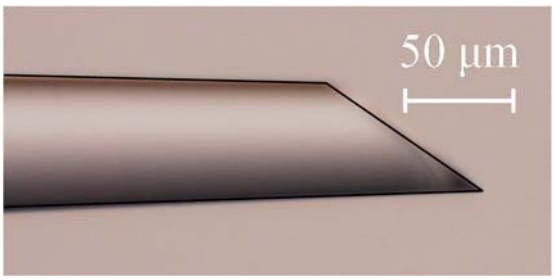

Figure 2. Zoom view of the probe tip.

Figure 3 shows a typical output signal of a single droplet measurement by the S-TOP. First, the gas-phase level V_{Gas} and the liquid-phase level V_{Liquid} were determined (Sakamoto and Saito 2011). Second, the high- and low-threshold levels, V_{thh} and V_{thl}, were selected (see Section 3.2). Finally, the gradient of the leading edge through the V_{thh} (P1) and V_{thl} (P2) was calculated by equation (1).

$$g_{rd} = \frac{dV}{dt}\frac{1}{(V_{Gas}-V_{Liquid})} \quad . \tag{1}$$

The droplet velocity U_D (in a strict sense, the average interface velocity of a droplet during measurement) was calculated from,

$$U_D = \alpha \times g_{rd} \quad , \tag{2}$$

where α is a proportionality constant between the interface velocity and g_{rd} (Fig. 4, obtained by preliminary penetration experiments [Mizushima and Saito 2012]). The measured chord length L_D was calculated as follows,

$$L_D = U_D \times (t_f - t_s) \quad , \tag{3}$$

where t_s and t_f are the starting and finishing time of the S-TOP's contact with a droplet. The time, t_s, is defined as the intersection point of the straight line (i.e., the gradient is g_{rd}), and the gas phase level at the leading edge. Meanwhile, t_f is defined as the time at which a "post-signal" takes the maximum value (see Section 3.2). t_f was determined by using a biphasic method [e.g., Achleitner,U., et al. 2001].

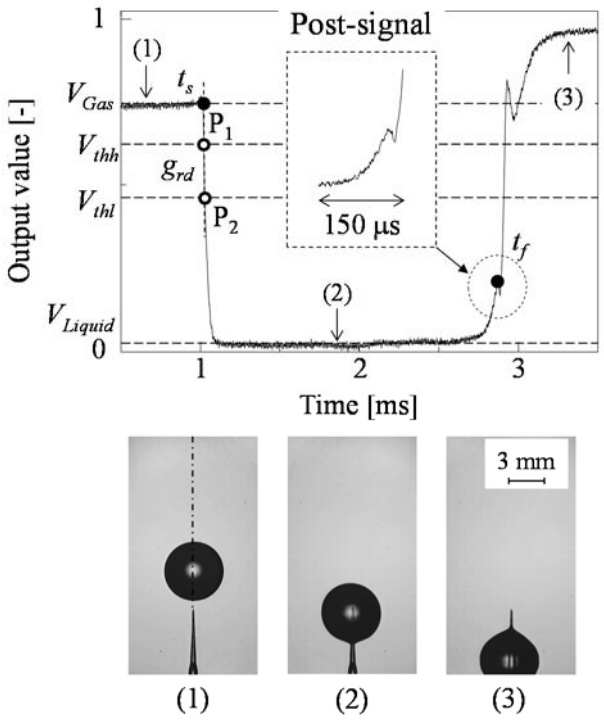

Figure 3. A typical signal of the S-TOP, in droplet measurement.

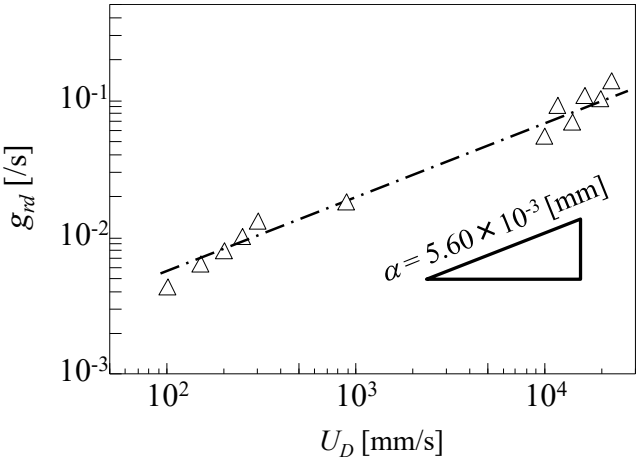

Figure 4. Relationship of U_D and g_{rd}.

3. Analysis of the signal from the S-TOP

3.1. 3D ray-tracing simulation

In this study, we interpret the S-TOP signal using a 3D ray-tracing simulation. Ray tracing is a technique for rendering images with computers. The idea behind ray tracing is that physically correct images are composed by light, and that light will usually come from a light source and bounce around (i.e., reflect) as light rays in a scene before hitting our eyes or a camera. The probe signal is also led by reflection. By reproducing in a computer simulation the path followed from a light source to a photo multiplier, we are able to produce physically relevant meanings of the signal.

Cartellier and Barrau (1998) carried out 2D ray-tracing simulation for optimizing the sensing tip of a mono-fiber optical probe. Sakamoto and Saito (2012) developed 3D ray-tracing simulation for analyzing signals of the S-TOP, and this simulator was in good accord with experiment results. In addition, the non-axial symmetry of the S-TOP invoked very hopeful and unique phenomena.

A light wave propagating in the fiber was simplified as discrete ray segments. Conditions of the target optical setup of the S-TOP are: that there be no magnetized object; that the step-index optical fiber be homogeneous and lossless; and, that the probe diameter (inlet tip: 230 μm, sensing tip: 60 μm) be a sufficient amount larger than the source light wavelength (650 nm). The path and energy of the rays were calculated by considering the incident angles and refractive indices of the mediums. The path of a reflecting/refracting ray was calculated as a vector in consideration of a reflection/refraction angle. The reflection angle is the same as the incident angle. The refraction angle is given by Snell's law,

$$\frac{\sin\theta_t}{\sin\theta_i} = \frac{n_i}{n_t} \quad , \tag{4}$$

where θ_i, θ_t, n_i, n_t are the incident angle, the refracting angle, the refractive index of the incoming media, and the refractive index of the transmitting media, respectively.

The energy of a reflecting/refracting ray was calculated from the reflectivity/transmissivity governed by Fresnel's equation,

$$R_P = \frac{\tan^2(\theta_i - |\theta_t|)}{\tan^2(\theta_i + |\theta_t|)} , \quad (5)$$

$$R_S = \frac{\sin^2(\theta_i - |\theta_t|)}{\sin^2(\theta_i + |\theta_t|)} , \quad (6)$$

where R_P and R_S are reflectivities of parallel and perpendicular polarization, respectively; for transmissivity,

$$T_P = \frac{\sin(2\theta_i)\sin(2|\theta_t|)}{\sin^2(\theta_i + |\theta_t|)\cos^2(\theta_i - |\theta_t|)} , \quad (7)$$

$$T_S = \frac{\sin(2\theta_i)\sin(2|\theta_t|)}{\sin^2(\theta_i + |\theta_t|)} , \quad (8)$$

where T_P and T_S are the transmissivities of parallel and perpendicular polarization, respectively. Here, we assume that the interfaces are optically smooth enough to neglect random reflection. All the ray energy that returns from the sensing tip was summed up as the output voltage.

Figure 5 is a flow chart of this computation. The objects of the computation were categorized and rendered into three primitive types: BODY, SURFACE, and RAY. Every object possessed particular information that corresponded to the optical phenomena of the S-TOP system and was needed for the ray-tracing calculation; i.e., a BODY had a homogeneous refractive index, a SURFACE had its 3D shape information, and a RAY had its root point and direction. Owing to good linkage among the objects, the computational cost was successfully lowered. Moreover, we were able to easily track the history of every light path and energy in the fiber.

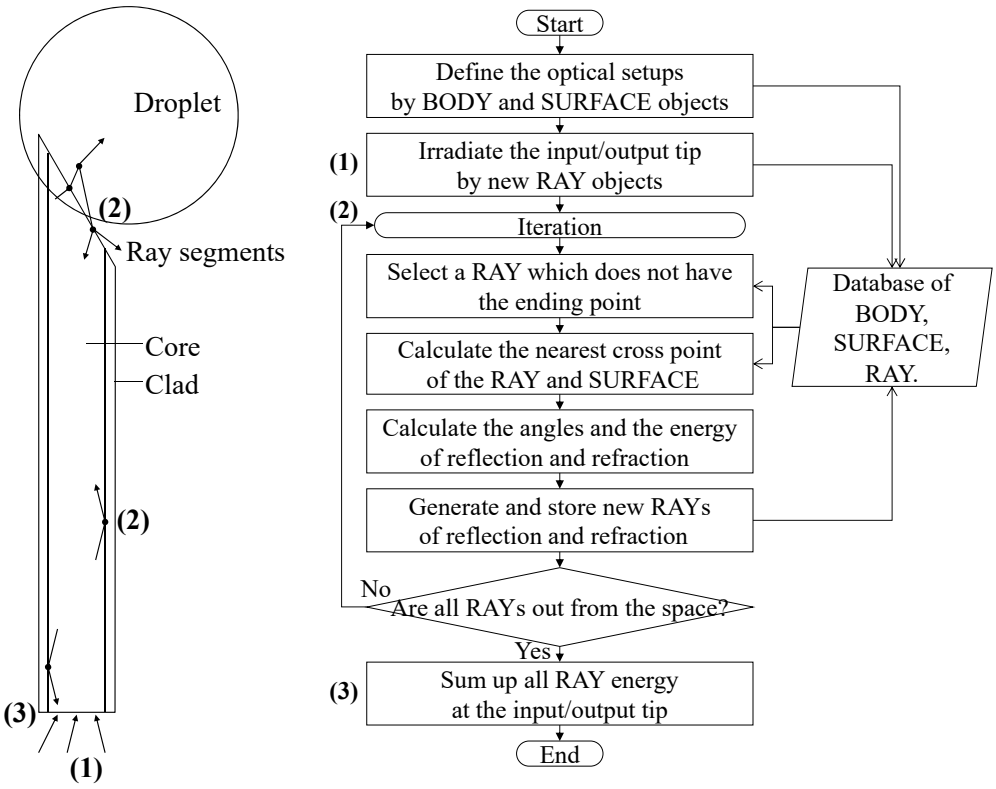

Figure 5. Flow chart of the 3D ray-tracing simulation.

3.2. Signal analysis and sensitivity length

3.2.1 On/off signal

In this section, we analyze the S-TOP signals based on the simulation results. At point (1) in Fig. 3 (a), the sensing tip is in the air phase. Some beams reaching the sensing tip reflect and return due to the large difference in the refractive indices of the fiber (1.46) and air (1.00). About 2% of the inlet rays are detected as the air-phase level (V_{Gas}). At point (2), the S-TOP penetrates the droplet, and the tip is positioned in liquid. Less than 0.01% of the inlet rays are return beams, and the rest are discharged into the water phase due to the small difference in refractive indices of fiber (1.46) and water (1.33); as a result, the output level drops to almost zero (V_{Liquid}). At (3), the S-TOP finishes piercing the droplet, and the sensing tip is positioned in the air phase again. The output returns to the

air-phase level. Thus, an on/off signal is obtained. Many researchers have been trying to maximize the V_{Gas}/V_{Liquid} ratio to minimize the influence of the probe presence on flows and to measure smaller bubbles by shaping the sensing tip into a U-type, convex-type, prism-link-type, cone-type, or wedge-type (Cartellier 1991).

To provide the validity of these types of optical fiber probe, the sensitive length, L_s, of the probe is important, a notion first introduced by Cartellier (1990). L_s is the length over which the probe provides most of the voltage change during the penetration. Figure 6 shows the relationships between I (the light intensity distribution contributing to V_{Gas}), V (the output value of the S-TOP), and h (the distance from the S-TOP tip). I is the result of the ray-tracing simulation. V_{gas} is described with I and h,

$$V_{Gas} = \int_0^1 I(h)dh \quad . \tag{9}$$

When the interface moves up a distance of x from the tip, V is calculated as

$$V(x) = V_{Gas} - \int_0^x I(h)dh \quad . \tag{10}$$

The gradient of V is largest in the area from Q_1 to Q_2, where the most intensive light contributing to V_{Gas} is distributed. $V|_{at\ Q1}$ and $V|_{at\ Q2}$ correspond to 80% and 60% of the $V_{Gas}-V_{Liquid}$ amplitude, respectively. Here, $V|_{at\ Q1}$, $V|_{at\ Q2}$, and the length of the Q_1Q_2 segment are the high- and low-threshold value (V_{thh} and V_{thl} were thus defined) and L_S. L_S indicates the spatial resolution; therefore, it should be smaller than the measurement object. In this study, L_S of a wedge-shaped tip is expressed by α (= 5.6 μm) in Eq. (2). This is a favorable value for the measurement of submillimetre droplets.

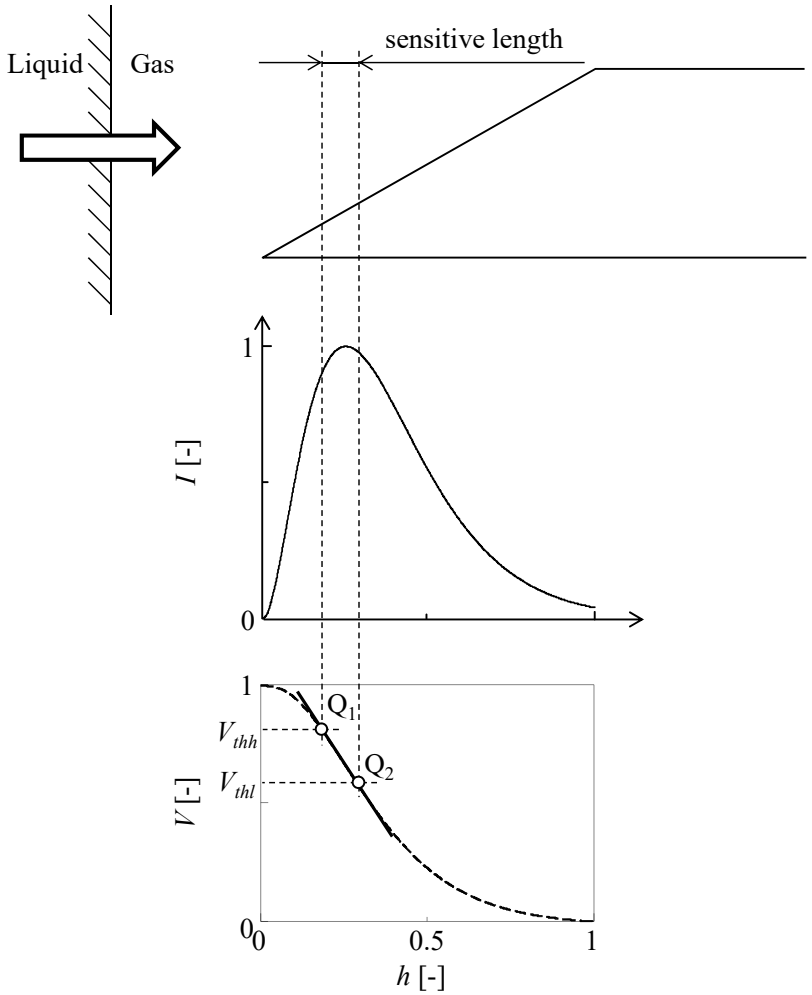

Figure 6. Sensitivity length of the S-TOP.

3.2.2 Post-signal

In the inset of Fig. 3, a small peak is found after the S-TOP pierces a droplet (i.e., before the S-TOP pierces the droplet rear surface); we call this a post-signal. A typical computation result of the post-signal is shown in Figure 7. Fig. 7 (i) is a calculated output signal of the S-TOP. At point (b), the post-signal shows a short peak, as in the experiment. In tracking the history of the light path contributing to the post-signal, we discovered that the output signal is a superposition of the on/off signal (Fig. 7 [ii]) and the post-signal (Fig. 7 [iii]). Clearly, the former is reflected light at the sensing tip and the latter is reflected light at the rear interface of the droplet. According to Fig. 7 (iii), the reflected

light at the rear interface re-enters the S-TOP before the S-TOP finishes piercing the droplet. After the tip touches the droplet rear surface, a meniscus is formed around the S-TOP tip. As a result, the intensity of the re-entered light decreases. Hence, the time of the peak exactly indicates the finishing time of a droplet measurement (t_f was thus defined).

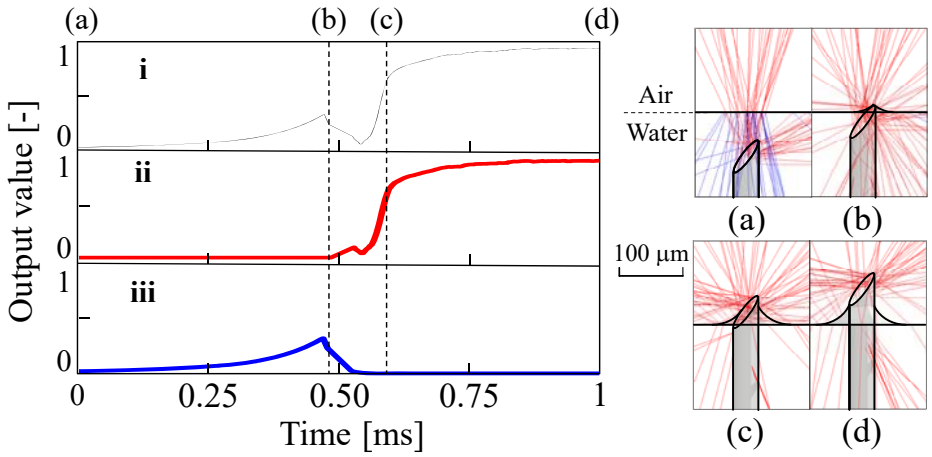

Figure 7. Simulation result of the S-TOP penetrating the gas-liquid interface from the water to the air.

The post-signal gives us information not only on the accurate event time but also on the contact positions of the S-TOP on the droplet. According to Eq. (3), the chord length obtained by the S-TOP is very similar to the droplet's minor axis when it pierces the center region of the droplet. However, chord length depends entirely on the touch position on a droplet; therefore, it is very difficult to measure a droplet's axial length in a droplet flow. Hong et al. (2004) conducted a statistical correction for the error of droplets' axes measured through a mono-optical probe. They analyzed signal responses in various droplet conditions (droplet size and incoming position or angle of probe), improved their signal processing, and progressed to successful measurement of the droplet with OFP. The post-signal is very useful for improving the robustness and reliability of droplet measurement with an OFP. This signal takes the largest value, when the interface against the S-TOP axis is "flat" (i.e., the center region of the spherical droplet). Next, we

experimentally quantify the relationship between S-TOP touch positions and the intensities of the post-signal.

3.2.3 Description of experiments

Figure 8 is a schematic diagram of the experimental setup. Ion-exchanged water was introduced into a cylinder and pressurized. Single droplets were injected from a micro capillary ([h]; 140-μm inner diameter) placed 10 cm above the S-TOP (a). Free-falling droplets were measured with the S-TOP fixed on a three-axis microstage, at controlled touch positions of L_{probe}/L_{major} = 0, 10, 30, 45%, respectively (Figure 9). The average equivalent diameter of the droplets was about 2.0 mm, and their average velocity was about 1.0 m/s. We visualized the process of the droplets pierced by the S-TOP using a high-speed video camera ([e]; frame rate 10000 fps, exposure time 50 μs, resolution 1024×512 pixels, and spatial resolution 8.33 μm/pixel) and a halogen light (g).

4. Results and Discussion

Figure 10 shows output signals obtained from the measurements and corresponding images. Table 1 lists the measurement results for droplet velocities and pierced chord lengths. These signals were similar; however, the measured chord lengths were very different.

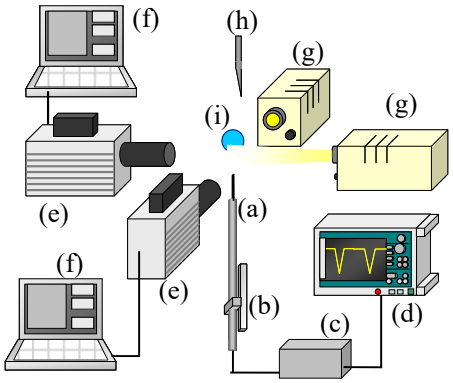

(a) Probe, (b) Optical stages, (c) Optics, (d) Data logger (e) High-speed video cameras, (f) PC, (g) Halogen light, (h) Needle, (i) Droplet

Figure 8. Experimental setup for droplet measurement.

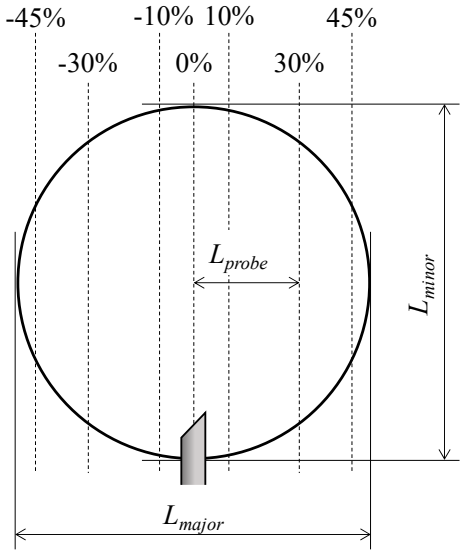

Figure 9. Conditions of the piercing position in the experiments.

The touch positions are defined as L_{probe}/L_{major} (L_{probe}: the distance from the droplet minor axis to the touch position of the S-TOP, L_{major}: the length of droplet major axis).

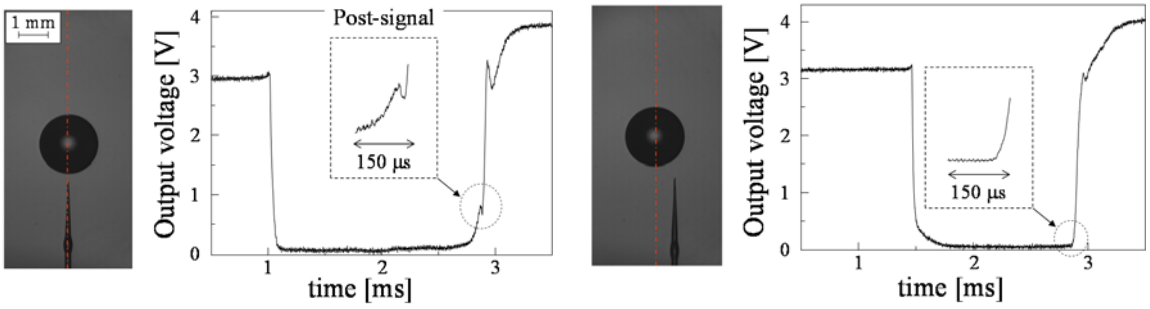

(a) Center region (L_{probe}/L_{major} = 0%) (b) Outer region (L_{probe}/L_{major} = 30%)

Figure 10. Output signals in the experiment.

Table 1. Difference in measurement results of the S-TOP and visualization.

(a) Velocity measurements

Touch Position [%]		0	10	30	45
Velocity [m/s]	$U_{S\text{-}TOP}$	0.91	0.89	0.82	0.81
	$U_{visualization}$	0.95			
Difference [%]		4	7	14	15

The touch position is defined on page 13 and Figure 9.

$U_{S\text{-}TOP}$: The average velocity measured through the S-TOP.

$U_{visualization}$: The average velocity measured through the high-speed visualization.

"Difference" is defined by $|U_{visualization} - U_{S\text{-}TOP}|/U_{visualization}$.

(b) Size measurements

Touch Position [%]		0	10	30	45
Pierced chord length	L_D	1.68	1.66	1.17	0.61
Minor axis measured through visualization	L_{Minor}	2.0			
Difference [%]		16	17	41	69

L_D: The average chord length pierced by the S-TOP.

L_{Minor}: The average length of minor axis measured through the high-speed visualization.

"Difference" is defined by $|L_{Minor} - L_D|/L_{Minor}$.

Experimental results of the relationship between the post-signal intensity and the touch position are plotted in Figure 11. The post-signal clearly reached a peak around the center region (L_{probe} / L_{major} < 5%). Under the other conditions, post-signals were not detected. This fact accorded with the intensity distribution of post-signals numerically simulated (Figure 12). Apparently, the post-signal sharply peaks at the center region and decreases rapidly with shifts toward the outer region.

The reason why the post-signal intensity appears only when the S-TOP touches the center region of a droplet is explained geometrically. Figure 13 (a) is a numerical result of the spatial distribution of light energy of discharged beams from the S-TOP tip to the surrounding water. The discharged beams have directional characteristics against the S-TOP axis. When the S-TOP touches a droplet interface almost perpendicularly, as shown in Figure 13 (b), beams reflected at the interface are effectively collected. On the other hand, the beams are immediately reflected off of the S-TOP axis when the interface inclines (i.e., the pierced position moves from the center region) (Figure 13 [c]). These tendencies apply to arbitrary spherical or spheroidal droplets. These tendencies apply to arbitrary spherical or spheroidal droplets. We normalized output signals after determining the gas-phase (air phase) level and the liquid-phase (water phase) level by using the histogram method and the median method [Sakamoto and Saito 2012]. We automatically obtained the corresponding normalized threshold level of the post-signal in proportional allotment. In addition, on the basis of preparatory experiments' results and the 3D ray-tracing simulation performed under the same conditions as those used for the experiments, the uncertainty of the normalized post-signal intensity was estimated at approx. ±2%.

If the post-signal appears, we immediately know that the S-TOP has touched a droplet at the vicinity of its pole (L_{probe}/L_{major} < 5%), and can calculate the velocity and chord length. Inversely, if no post-signal appears in an S-TOP signal, we can understand that the signal is insufficient for correct measurement due to an incomplete piercing condition and ignore the signal as null.

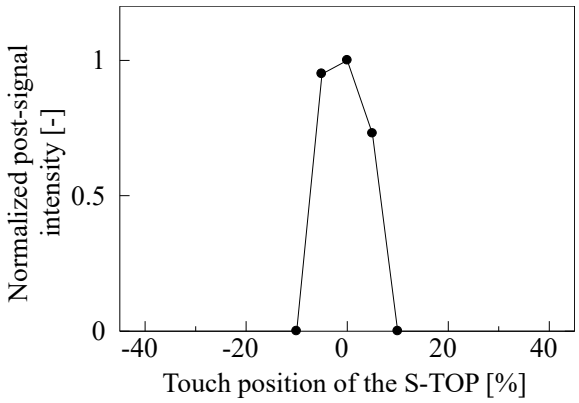

Figure 11. Relationship between the post-signal intensity and touch position.

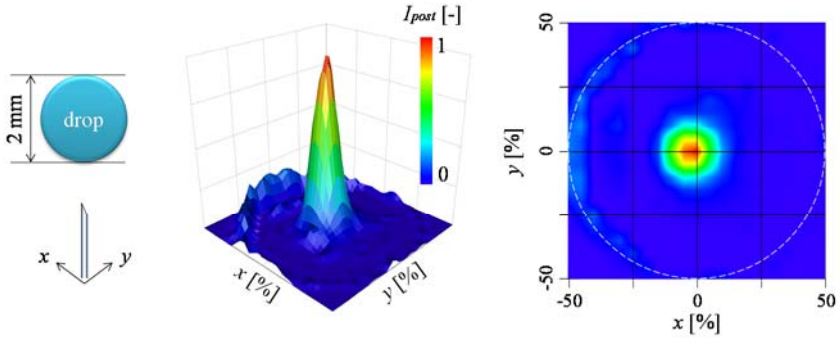

Figure 12. Intensity distribution of the post-signal using the 3D ray tracing simulation (I_{post} is a normalized post-signal intensity).

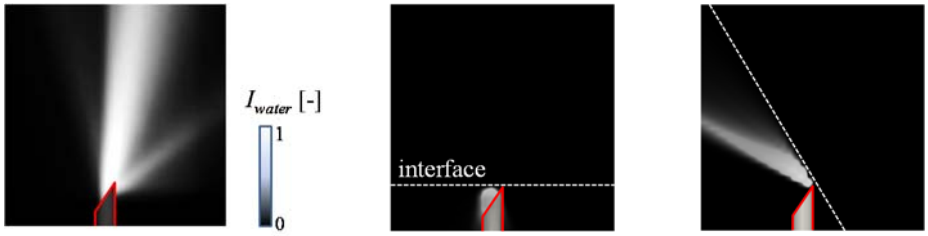

Figure 13. Intensity distribution of the discharged beams from the S-TOP tip to surrounding water (I_{water} is a normalized discharged beam intensity), and reflection off the inner interface of the droplet.

According to Table 1 (a), the post-signal measurement promises accurate velocity measurement within ± 5% uncertainty. This kind of uncertainty was discussed in our

previous studies (Mizushima and Saito 2012), and we contend that it should be considered within an allowance. In the diameter measurement of a droplet by the optical fiber probe, the uncertainty raised by the randomness of the touch position; in addition, the penetration angle was large (as shown in Table 1 (b)). In order to numerically analyze this uncertainty and to numerically demonstrate the effect of the post-signal method, we performed a 3D ray-tracing simulation with consideration of the Monte-Carlo method (Fig. 14a). In this analysis, the droplet diameter was given from 1 mm to 1.5 mm randomly, and the normalized touch position (L_{probe}/L_{major}) was also given from 0% to ±45% randomly. The penetration angle was given randomly from 0° to ±15°. Figure 14 shows the results of the above numerical simulation for discussing the uncertainty of the chord length measurement. Using the post-signal method, L_{minor}/L_D is remarkably reduced from 30% to less than 3%. Reliable sample sizes for these values are also enhanced from 200 to 10 droplets, which suggests the high degree of accuracy of this new method. Note that this discussion does not include the uncertainty of droplet motions (oscillation and deformation) during measurement. In fact, the difference of L_D and L_{minor} essentially remains 10% even at the center region (Table 1 [b]) due to random oscillations of the droplet (Saito et al. 2009). The remainder of the difference is attributed to bias errors of the velocity measurement and surface deformation during piercing (Mizushima and Saito 2012).

The post-signal method is qualified to measure for spherical or spheroidal droplets in the flow. According to Clift et al., if interfacial tension and/or viscous forces are much more dominant than inertia forces, a droplet will stably shape into a sphere at moderate Reynolds number (e.g., $Re < 600$; droplets falling freely in systems of practical importance). In this case, the droplet size must be measured within 5% uncertainty (bias error) only due to the surface deformation. In this study ($Re = 2000$), an uncertainty of 10% essentially remains in L_D, because although the droplet keeps the shape of a sphere, it becomes slightly instable. Hence, we can measure droplet sizes to within 10%

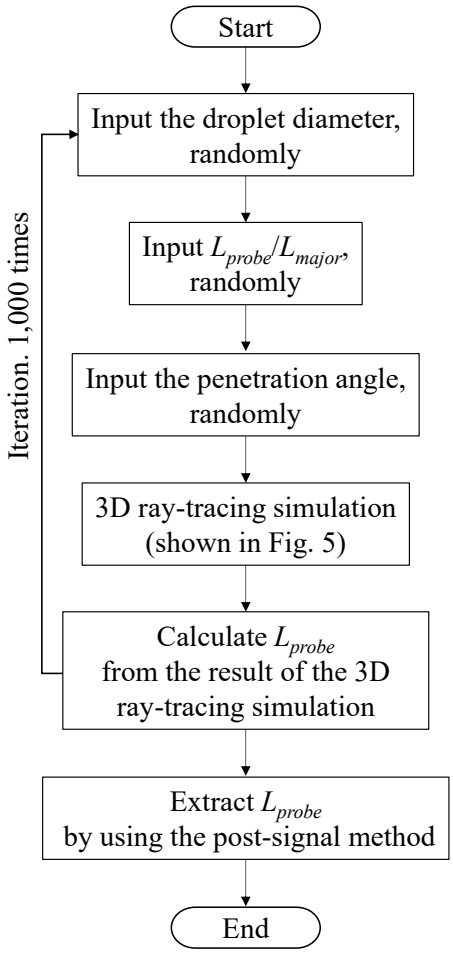

Figure 14 (a). Flow chart of the 3D ray-tracing simulation with consideration of Monte-Carlo method.

accuracy in a droplet flow of $Re \leq 2000$ only by using the post-signal method. Provided that the droplet shapes are a sphere or spheroid (diameter range in an air-water system: approximately 50 μm – 3 mm), the post-signal method is helpful to OFP measurements.

Conventional multi-tip optical fiber probes such as a four-tip optical fiber probe affect the droplet velocity due to their high resistance at the piercing of a droplet, and their multiple piercings deform the droplet shape. It is also very difficult for these probes to detect the touch position. Our new method has a smaller effect on the droplet velocity, providing less deformation of the droplet shape and the accurate detection of the touch position. The detection of the touch position has long been the most difficult problem to

solve. S-TOP with this new method (which we have named the "post-signal method") enables the accurate measurement of small droplets, which have been difficult to measure with the conventional multi-tip optical fiber probes. We have demonstrated the good performance of the post-signal method. This new method is very simple, but more effective than any other statistical approach.

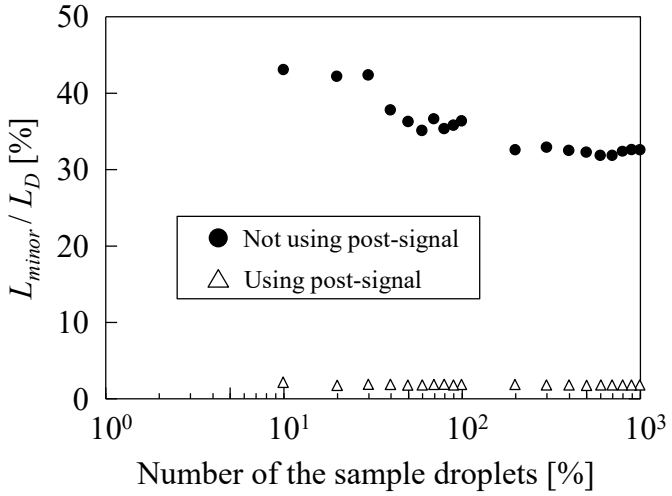

Figure 14 (b). Variation of measured chord lengths based on Monte-Carlo simulations.

Concluding remarks

Our purpose was to improve the accuracy of droplet measurement through the S-TOP. We carefully analyzed output signals of the S-TOP, using 3D ray-tracing simulation, and discovered a potentially useful relationship between the intensity of the post-signal and the S-TOP's touch position on a droplet. The post-signal intensity peaked when the S-TOP touched the center region of a droplet. Applying these overlooked characteristics to signal processing in S-TOP measurement, we established the post-signal method. We then worked continuously to improve the S-TOP's measurement accuracy, e.g., by identifying whether the S-TOP had touched a droplet at the vicinity of its pole or not. This newly developed method can reduce the difference between the measured chord length and the

length of the minor axis of a droplet remarkably, even in a dispersed flow. In addition to touch position detection, finding the peak of the post-signal is a reasonable indication of t_f (finishing time of the S-TOP's contact with a droplet). Consequently, we can measure the droplet sizes to within 10% accuracy in the droplet flow of $Re \leq 2000$. More quantitative study of the limitations of this new method is needed. Despite a limited range of applicability, the post-signal method has robust potential for the inevitable problems of OFP measurement in practical droplet flows.

Nomenclature

g_{rd}	gradient of the S-TOP signals (1/s)
h	dimensionless distance from the S-TOP tip (dimensionless)
I	light intensity of the beams returned from the S-TOP tip (dimensionless)
I_{water}	normalized discharged beam intensity from the S-TOP tip positioned in water (dimensionless)
I_{post}	normalized post-signal intensity (dimensionless)
L_D	pierced chord length of S-TOP (mm)
L_{major}	length of droplet major axis (mm)
L_{minor}	length of droplet minor axis (mm)
L_S	sensitive length of S-TOP (μm)
L_{probe}	distance from the droplet minor axis to the touch position of the S-TOP (mm)
n	refractive index (dimensionless)
P	end of line segment (dimensionless)
Q	end of line segment (dimensionless)
R	reflectivity (dimensionless)

t	time (s or ms)
T	transmissivity (dimensionless)
U	velocity (m/s)
V	output value of the S-TOP signal (dimensionless)
x	arbitral value of h (dimensionless)

Greek symbols

α	proportionality coefficient (mm)
θ	degree (deg.)

Subscripts

D	droplet
f	end of touch
G	gas phase
Gas	gas-phase level
i	incident ray
I	gas–liquid interface
L	liquid phase
Liquid	liquid-phase level
P	p-polarization
s	start of touch
S	s-polarization
t	transmit ray
thh	high threshold level
thl	low threshold level

Abuaf, N., Jones. O. C. Jr., and Zimmer. A.; Optical probe for local void fraction and

interface velocity measurements, *Rev. Sci. Instrum.*, **49**, 1090-1094 (1978)

Achleitner,U., Rheinberger, K., Furtner, B., Amann, A. and Baubin, M.; Waveform analysis of biphasic external defibrillators, Resuscitation, **50**, 61-70 (2001).

Aprin, L., Mercier, P. and Tadrist, L.; Experimental analysis of local void fractions measurements for boiling hydrocarbons in complex geometry, *Int. J. Multiph. Flow*, **33**, 371-393 (2007)

Barrau, E., Riviere, N., Poupot, C. and Cartellier. A.; Single and double optical probes in air-water two-phase flows: real time signal processing and sensor performance, *Int. J. Multiph. Flow*, **25**, 229-256 (1999)

Cartellier, A., Optical probes for local void fraction measurements: characterization of performance, *Rev. Sci. Instrum.*, **61**, 874-886 (1990)

Cartellier, A.; Local phase detection probes in fluid/fluid two-phase flows, *Rev. Sci. Instrum.*, **62**, 279-303 (1991)

Cartellier, A. and Barrau, E.; Monofibre optical probes for gas detection and gas velocity measurements: conical probes, *Int. J. Multiph. Flow*, **24**, 1265-1294 (1998)

Clift, R., Grace, J. R. and Weber. M. E.; Bubbles, Drops and Particles, *Academic Press New York* (1978)

Harteveld, W. K., Bubble columns - structure or stability?, *PhD thesis of TU Delft* (2005)

Hess, C. F.; Planar Particle Image Analyzer, *9th. Int. Symp. Applications of Laser Techniques to Fluid Mechanics*, Lisbon-Portugal 18.1 (1998)

Higuchi, M. and Saito, T.; Quantitative characterizations of long-period fluctuations in a large-diameter bubble column based on point-wise void fraction measurements, *Chem. Eng. J.* **160**, 284-292 (2010)

Hong, M., Cartellier, A. and Hopfinger, E. J.; Characterization of phase detection optical probes for the measurement of the dispersed phase parameters in sprays, *Int. J. Multiph. Flow*, **30**, 615-648 (2004)

Kawaguchi, T., Akasaka, Y. and Maeda, M.; Size measurements of droplets and bubbles

by advanced interferometric laser imaging technique, *Meas. Sci. Technol.*, **13**, 308-316 (2002)

Miller, N. and Mitchie, R. E.; Measurement of local voidage in liquid/gas two-phase flow systems, *J. Brit. Nucl. Energy Soc.*, **2**, 94 (1970)

Mizushima Y and Saito T 2012 Detection method of a position pierced by a single-tip optical fibre probe in bubble measurement Meas. Sci. Technol. 23 085308

Saito, T., Matsuda. K., Ozawa, Y., Oishi, S. and Aoshima, S.; Measurement of tiny droplets using a newly developed optical fiber probe micro-fabricated by a femtosecond pulse laser, *Meas. Sci. and Technol.*, **20**, 114002 (2009)

Sakamoto, A. and Saito, T.; Robust algorithms for quantifying noisy signals of optical fiber probes employed in industrial-scale practical bubbly flows, *Int. J. Multiph. Flow*, **41**, 77-90 (2012)

Sakamoto, A. and Saito, T.; Computational analysis of responses of a wedge-shaped-tip optical fiber probe in bubble measurement, *Rev. Sci. Instrum.*, **83**, 075107 (2012)

Sommerfeld, M. and Qiu, H. H.; Characterization of particle-laden, confined swirling flows by phase-doppler anemometry and numerical calculation, *Int. J. Multiph. Flow*, **19**, 1093-1127 (1993)

Vejrazka, J., Vecer, M., Orvalho, S., Sechet, P., Ruzicka, M. C. and Cartellier, A.; Measurement accuracy of a mono-fiber optical probe in a bubbly flow, *Int. J. Multiph. Flow*, **36**, 533-548 (2010)

Xue, J.; Bubble Velocity, Size and Interfacial Area Measurements in Bubble Columns, *PhD thesis of Washington University*, (2004)